Extreme waves induced by strong depth transitions: Fully nonlinear results

Claudio Viotti and Frédéric Dias

Citation: Physics of Fluids (1994-present) **26**, 051705 (2014); doi: 10.1063/1.4880659
View online: http://dx.doi.org/10.1063/1.4880659
View Table of Contents: http://scitation.aip.org/content/aip/journal/pof2/26/5?ver=pdfcov
Published by the AIP Publishing

PHYSICS OF FLUIDS **26**, 051705 (2014)

Extreme waves induced by strong depth transitions: Fully nonlinear results

Claudio Viotti[1] and Frédéric Dias[1,2]
[1]*School of Mathematical Sciences, University College of Dublin, Dublin, Ireland*
[2]*CMLA, ENS Cachan, France*

(Received 13 January 2014; accepted 1 May 2014; published online 29 May 2014)

Recent studies on free-surface gravity waves over uneven bathymetries have shown that "rogue" waves can be triggered by strong depth variations. This phenomenon is here studied by means of spectral simulations of the free-surface Euler equations. We focus on the case of a random, one-directional wave field with prescribed statistics propagating over a submerged step, and consider different depth variations, up to an almost deep-to-shallow transition ($k_pH \approx 1.8 - 0.78$, where k_p is the characteristic wavenumber and H the water depth). Strongly non-Gaussian statistics are observed in a region localized around the depth transition, beyond which they settle rapidly on the steady statistical state of finite-depth random wave fields. Extreme fluctuations are enhanced by stronger depth variations. Freak-wave formation is interpreted as a general signature of out-of-equilibrium dynamics, associated with the spectral settling from the deep-water to the finite-depth equilibrium. We also document that during such a transition the wave spectrum shows remarkable similarity with Phillips ω^{-5}-law for the strongest depth variations considered. © *2014 AIP Publishing LLC*. [http://dx.doi.org/10.1063/1.4880659]

Rogue waves represent a fascinating and challenging research subject. A variety of physical mechanisms have been proposed as candidates for explaining the rare yet striking observations of rogue waves in the ocean;[1,2] which mechanisms are more "realistic," i.e., likely to occur spontaneously in nature, is a subject of ongoing debate. The propagation of waves over strong depth variations, in particular, has been recognized as a favorable condition for the occurrence of extreme waves,[3] and is receiving growing attention in such context. From the modeling view point, Zeng and Trulsen[4] approached the problem in the context of the nonlinear Schrödinger equation, therefore within the limit of a slowly varying bottom. The prediction obtained in such theoretical framework showed a transition between two statistically steady states on each side of the depth transition, but it did not allow to observe the enhanced probability of extreme wave events that experimental observations revealed.[3] Gramstad *et al.*[5] and Sergeeva *et al.*[6] obtained trends qualitatively similar to the experimental data using one-directional Boussinesq[5] and Korteweg-de Vries (KdV)[6] models. In particular, they document the emergence of extreme-wave activity near the shallow side of bottom slopes.

Although the above studies have provided valuable insight into the wave dynamics over variable bathymetry from the standpoint of extreme wave formation, there is a clear need to extend the mathematical and numerical modeling to the fully nonlinear case. Furthermore, due to the shallow water assumption, previous studies could not assess the relevant case of deep- to shallow-water transitions. The present study therefore aims to provide the first, fully nonlinear numerical study on the same physical setup. We take advantage from the ease in varying parametrically the bathymetric profile in a way that would be impractical to realize in experiments, and from the nearly complete removal of measurement noise which allows to observe the high-frequency tail of the wave spectrum.

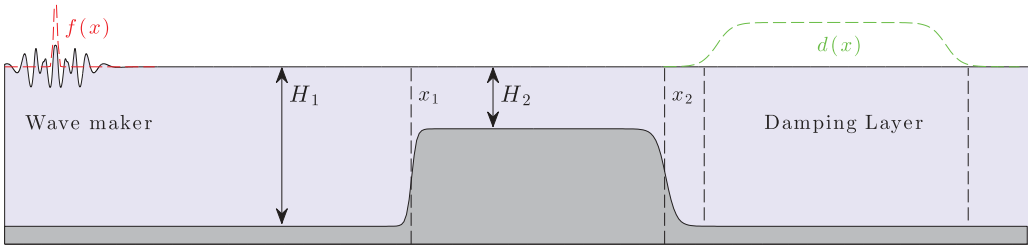

FIG. 1. Schematic of the numerical setup employed, showing the regions where the forcing and damping terms are located.

By assuming irrotational flow and neglecting surface tension, the free-surface Euler system in two spatial coordinates (x, y) and time t reads

$$\eta_t = -\phi_x \eta_x + \phi_y, \qquad \text{at} \quad y = \eta(x,t), \tag{1}$$

$$\phi_t = -\tfrac{1}{2}\left(\phi_x{}^2 + \phi_y{}^2\right) - g\eta + P_F/\rho - P_D/\rho, \quad \text{at} \quad y = \eta(x,t), \tag{2}$$

$$\nabla\phi \cdot \mathbf{n} = 0, \qquad \text{at} \quad y = b(x), \tag{3}$$

$$\nabla^2\phi = 0, \qquad \text{for} \quad b(x) < y < \eta(x,t), \quad 0 < x < L, \tag{4}$$

where $\eta(x, t)$ is the free surface elevation, $\phi(x, y, t)$ is the velocity potential, $b(x) < 0$ is the bottom profile, ρ is the fluid density, g is the vertical acceleration due to gravity, $\mathbf{n}$ is the outward-pointing unit vector normal to the bottom profile, P_F and P_D are two pressure terms employed to introduce forcing and damping in the system, respectively, as discussed below. As we are going to apply a spectral discretization, we assume periodic boundary conditions in the horizontal x direction from the outset. This implies that η and $\nabla\phi$ (the fluid velocity) are periodic in x, whereas ϕ must be allowed to possess a non-periodic, linear part.

For the numerical solution of the system (1)–(4), we employ a spectral conformal mapping method extended to the case of variable bottom. For details we refer the reader to Viotti *et al.*[7] A well-known limitation of the potential-flow formulation lies in the assumption that no wave breaking occurs, which in practice limits the maximum wave steepness that one can consider. In the conformal-mapping method, wave breaking typically manifests as a dramatic loss of accuracy (which can be detected, for instance, as a significant violation of volume conservation), if not as a full breakdown of the computation. Therefore, it is necessary to seek for a compromise between the degree of nonlinearity and the numerical accuracy.

We intend to simulate a one-directional random wave field propagating toward a depth transition. In order to embed such a setup within a periodic computational domain, we employ a plateau-like bathymetric profile, and we introduce wave-maker and damping layer according to the configuration shown in Figure 1. In doing so, we effectively implement an inflow-outflow regime within the periodic domain.

The bottom bathymetry is defined as

$$b(x) = -H_1 + \tfrac{1}{2}(H_1 - H_2)\left[\tanh((x - x_1)/\delta_1) - \tanh((x - x_2)/\delta_2)\right],$$

where H_1 (H_2) is the depth of the deep (shallow) region, x_1 and x_2 are the centers of the depth transitions of thickness δ_1 and δ_2. In order to obtain the desired wave characteristics and avoid spurious effects, both wave generation and absorption need to be devised carefully. The wave-maker consists of a pneumatic generator

$$P_F(x,t)/\rho = f(x)N(t;\omega_0,\sigma_0),$$

characterized by a shape function $f(x)$, and a temporal law $N(t; \omega_0, \sigma_0)$, which is a Gaussian random process with power spectrum given by $P(\omega) = \frac{\mathcal{A}}{\sqrt{2\pi}\sigma_0}\exp\left[-\frac{1}{2}(\omega - \omega_0)^2/\sigma_0^2\right]$. The wave-maker peak frequency ω_0, bandwidth σ_0, and amplitude $\mathcal{A}$ are tuned in order to target a desired sea state with prescribed wave steepness and frequency. The shape function $f(x)$, is also shaped as a Gaussian,

with a thickness consistent with the typical wavelength associated with ω_0. The wave absorber is implemented as linear damping

$$P_D(x,t)/\rho = d(x)\phi\,(x,\eta(x,t),t)$$

localized by means of the shape function $d(x)$ (see Figure 1). The choice of d is delicate in relation to spurious effects such as wave reflection and pile-up. The latter consists of fluid accumulation inside the damping layer, and can alter significantly the water depth in the rest of the wave tank. Both effects are effectively reduced by distributing a weak damping over a large area, which clearly comes at the cost of reserving a consistent portion of the computational domain for the damping layer. Time series of the surface elevation are recorded on a grid of gauge locations along the tank. In order to ensure good resolution in frequency, we perform run-time data storage at every time step, furthermore, the conformal mapping method requires an interpolation every time η is evaluated at a given location in physical space. The time series produced in a single run contain about 1300 wave periods, accounting for the startup transient. We further average over two independent realizations. This appears sufficient for a satisfactory convergence of all statistical quantities considered in this study.

The medium being non-homogeneous, statistical quantities are defined locally in space. The sea state generated by the wave-maker is characterized by a local characteristic frequency ω_p (close but not equal to the wave-maker peak frequency ω_0), a corresponding wavenumber k_p that follows from the linear dispersion relation in finite depth $\omega_p^2 = gk_p \tanh k_p h$ (with $h(x) = -b(x)$), a spectral bandwidth Δ_ω, and an average steepness s, defined as

$$\omega_{\mathrm{p}} = \frac{\int_0^{+\infty} \omega S(\omega)\mathrm{d}\omega}{\int_0^{+\infty} S(\omega)\mathrm{d}\omega}, \quad \Delta_\omega^2 = \frac{\int_0^{+\infty} (\omega-\omega_{\mathrm{p}})^2 S(\omega)\mathrm{d}\omega}{\int_0^{+\infty} S(\omega)\mathrm{d}\omega}, \quad s = \sqrt{2}k_{\mathrm{p}}\eta_{\mathrm{std}},$$

where $S(\omega, x)$ is the power spectral density of the time series $\eta(x, t)$, $\eta_{\mathrm{std}} = \langle(\eta - \langle\eta\rangle)^2\rangle^{1/2}$ is the standard deviation of η (1/4 of the significant wave height, according to one common definition[1]), and $\langle\cdot\rangle$ denotes time-averaging. In order to characterize the emergence of extreme events, we also introduce skewness and kurtosis (or flatness) of the surface elevation, which are, respectively, given by

$$\lambda_3 = \langle(\eta - \langle\eta\rangle)^3\rangle/\eta_{\mathrm{std}}^3, \quad \lambda_4 = \langle(\eta - \langle\eta\rangle)^4\rangle/\eta_{\mathrm{std}}^4 - 3.$$

As is well known, for a Gaussian random process we have $\lambda_3 = \lambda_4 = 0$, which makes such high-order moments sensitive detectors of non-Gaussian features.

Before we proceed to showing the numerical results, we introduce a system of nondimensional units by normalizing upon the time scale $\tau = 1/\omega_0$ and the length scale $\ell = g/\omega_0^2$.

As a first case of study, we reproduce one of the experiments reported by Trulsen *et al.*,[3] which offers a good benchmark for our numerical method and setup. We choose the data set "case 1" in the above reference, since it realizes the closest condition to a deep- to shallow-water transition (the nominal values reported by Trulsen *et al.*[3] are $H_1 = 0.6$ m and $k_pH_1 = 1.6$ in the deep side, $H_1 = 0.3$ m and $k_pH_2 = 0.99$ in the shallow side). Experimental data are nondimensionalized upon $g = 9.8$ m/s^2 and $\omega_0 = 5$ s^{-1} (assumed equal to the nominal peak frequency reported in the same paper), and bathymetric parameters are also scaled accordingly. Numerical simulations are initialized from the quiescent state $\eta = \phi = 0$. Following the activation of the wave-maker, a statistically steady state in which the energy dissipated inside the damping layer balances the energy injected by the wave-maker, is attained in about 2000 dimensionless time units (≈300 wave periods), as shown in Figure 2(a).

A stringent yet physically meaningful criterion for assessing the overall numerical accuracy is offered by the amount of computational volume "leakage." In simpler setups, such as that of a soliton propagating over a submerged step, our scheme shows a clean exponential convergence. The trend reported in Figure 2(b) appears consistent with exponential accuracy at short times, whereas for long times the global accuracy appears somewhat degraded. This fact is not unexpected, as various sources of numerical error are present in the simulations which eventually pollute the nominal accuracy of the numerical scheme for long times. For instance, sharp-crested waves which appear as rare events

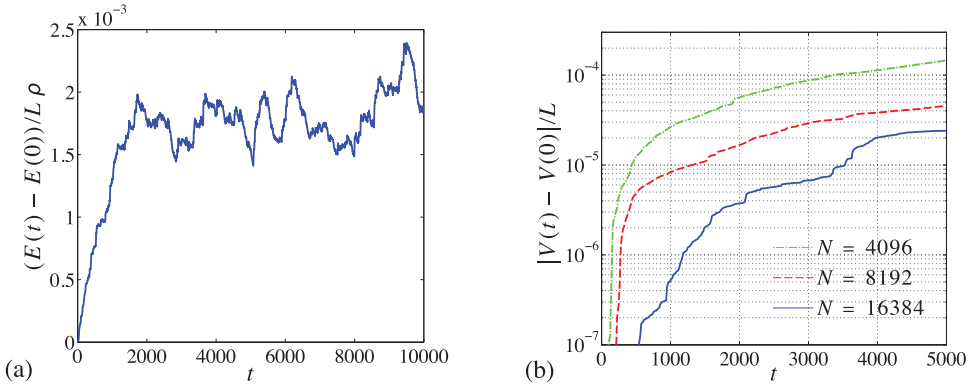

FIG. 2. Numerical replica of the "case 1" experiment reported by Trulsen *et al.*[3] (a) Time history of the total energy per unit length and unit density, from the wave-maker activation at $t = 0$ (for $N = 16\,384$). (b) Absolute volume variation per unit length versus time for different resolutions. N represents the number of dealiased Fourier modes employed. The total energy is given by $E = K + P = \frac{1}{2}\rho \int_0^L \int_b^\eta \left(\phi_x^2 + \phi_y^2\right) \mathrm{d}y\mathrm{d}x + \frac{1}{2}\rho \int_0^L \eta^2 \mathrm{d}x$, the total volume is given by $V = \int_0^L (\eta - b)\mathrm{d}x$.

are affected by larger numerical error at high frequency, and small truncation errors are introduced by the specific technique used to map the bathymetric profile in conformal space.[8] The discretization using $N = 16\,384$ (dealiased) Fourier modes provide a spectral resolution about 100 times larger than the characteristic wavenumber k_p. Based on this testing, we decided to employ this resolution in our simulations.

The x-dependent statistics obtained from our simulations are reported in Figure 3, along with the corresponding experimental data. The standard deviation (panel (a)) shows that we realized a very similar wave amplitude before the depth transition. The rightmost experimental data point suggests an attenuation of the significant wave height in the shallow side not present in the numerical simulation, but the experimental results are arguably affected by a certain amount of dissipation. Skewness (panel (b)) also matches accurately. In particular, the peak that occurs just beyond the depth transition is well resolved. In this regard, we observe a clear improvement with respect to the result obtained with a weakly nonlinear model.[5] Kurtosis (panel (c)) is also reproduced consistently, even though, as expected, it is affected by a larger statistical noise. In particular, the negative-kurtosis signature typical of intermediate-depth regimes[9] is evident.

The case just examined, even though insightful, shows only a moderate kurtosis enhancement. The other cases reported by Trulsen *et al.*[3] exhibit stronger freak wave activity, but are obtained by decreasing the wave frequency on the same bathymetry, whereby they consider the effect of the same depth variation on different upstream sea states. On the contrary, here we focus on the effect of different depth transitions with respect to a fixed upstream state. As such, we next focus on a new set of numerical experiments defined as follows. The total domain size is $L = 256\pi$, the water depth in the deeper region is kept constant $H_1 = 1.8$, while H_2 is varied in the range $0.55 < H_2 < 0.8$. We

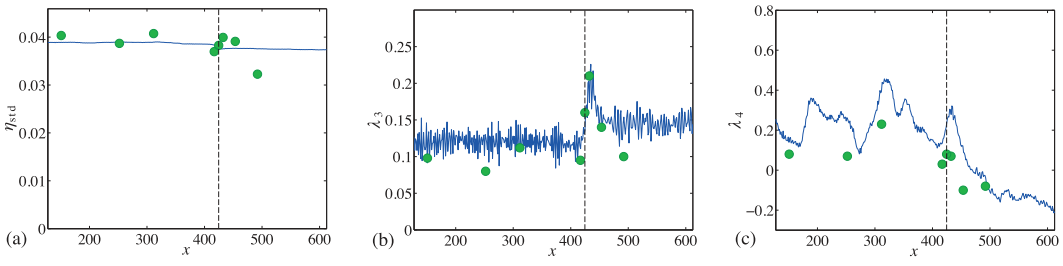

FIG. 3. Local wave field statistics for our simulation of the "case 1" experiment reported by Trulsen *et al.*:[3] (a) standard deviation, (b) skewness, and (c) kurtosis of the surface elevation. Lines: numerical results. Symbols: experimental data. Vertical lines reference the center of the depth transition $x = x_1$.

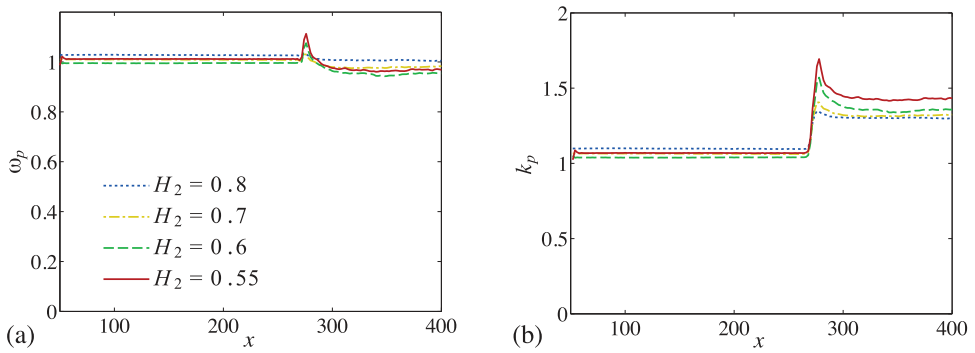

FIG. 4. (a) Characteristic frequency along the domain for the cases with $H_1 = 1.8$. (b) Characteristic wavenumber along the domain obtained from the linear finite-depth dispersion relation.

also set $x_1 = 270$ and $x_2 = 470$, with the corresponding thicknesses $\delta_1 = 2$ and $\delta_2 = 4$ (δ_2 is larger in order to minimize wave reflection from the second ridge). The parameters of the wave-maker are $\omega_0 = 1$ (by definition), and $\sigma_0 = 0.25$ for the bandwidth. For the damping, we use $\max(d(x)) = 0.05$.

In Figure 4, the x-dependent characteristic frequency and the associated wavenumber are reported. As shown, ω_p is very close to the forcing frequency $\omega_0 = 1$, and exhibits little spatial evolution in all the cases. On the contrary, k_p is slightly larger than 1 in the deep side (whereby we have $k_p H_1 \approx 1.8$), and increases in the shallow side. The regime attained within the shallower region therefore varies depending on H_2, namely, we obtain $k_p H_2 = 1.03, 0.92, 0.81, 0.78$ for $H_2 = 0.8, 0.7, 0.6, 0.55$, respectively. In these four cases, the deep-side sea is characterized by a spectral bandwidth $\Delta_\omega \approx 0.2$, and an average steepness $s \approx 0.068$. The associated Benjamin–Feir index $BFI \equiv s\omega_p/\Delta_\omega \approx 0.35$ corresponds to a subcritical regime ($BFI < 1$). This condition has been targeted on purpose, as it is typical of realistic sea states where modulational instability is saturated, and ensures a fast settling of the wave field on a near-Gaussian sea in the deep region. Furthermore, the absence of modulational effects in the deep-side sea allows to discern the non-Gaussian effects due to the depth transition, whereas a supercritical, narrow-banded sea state ($BFI > 1$) would likely produce non-Gaussian statistics due to nonlinear focussing.[8–12] The latter condition was discussed under the NLS equation by Zeng and Trulsen,[4] who observed a strongly non-Gaussian sea state developing upstream of the depth transition and then recovering near-Gaussian features in the shallow side, where nonlinear focussing is weak or absent altogether.

Further statistics are reported in Figure 5. The standard deviation η_{std}, panel (a), is essentially constant over the entire flume. Such a result can be understood from a classic argument based on the average energy-flux conservation. In the absence of dissipation, and assuming wave reflection is negligible, the mean, depth-averaged horizontal energy flux, $\overline{Q}$, is conserved throughout the wave tank. Since in a homogeneous wave field the energy flux can be estimated as $\overline{Q} \approx c_g E$ (see, e.g., Whitham[13]), where $E \approx \eta_{\text{std}}^2$ is the mean total energy per unit length, the variation of η_{std} is set by the variation of the group velocity corresponding to the characteristic frequency ω_p. However, as shown in Figure 5(d), $c_g(\omega_p)$ is weakly affected by the water depth if ω_p is sufficiently close to one (cf.

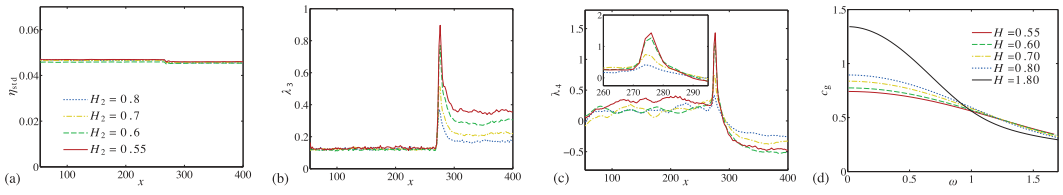

FIG. 5. Local wave field statistics for different depth variations (for $H_1 = 1.8$): (a) standard deviation, (b) skewness, and (c) kurtosis of the surface elevation. (d) Group velocity $c_g = \mathrm{d}\omega/\mathrm{d}k$ as a function of the wave frequency ω for different water depths H, from the nondimensional finite-depth dispersion relation.

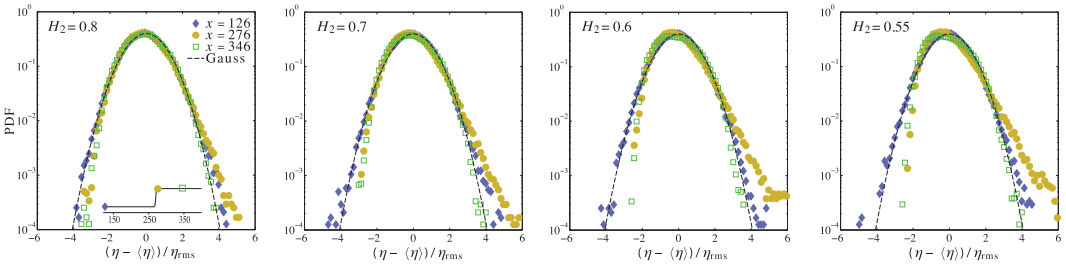

FIG. 6. Normalized PDFs of the free surface displacement at different x locations and for different depths H_2.

Figure 4), whereby the very mild variation of $\eta_{\rm std}$ appears consistent with the behavior of $\omega_p(x)$. In Figures 5(b) and 5(c), the local skewness and kurtosis for the same cases are shown. Spatial evolution is absent within the deep region for both quantities as the upstream sea state is in equilibrium, on the contrary strong fluctuations appear on the depth transition, denoting intensified freak-wave activity. New equilibrium conditions are then recovered downstream of the depth transition. These results are qualitatively similar to those reported in Figure 3 but the stronger depth variations here considered cause larger statistical anomalies. We observe that the peaks of skewness and kurtosis are sharply localized, whereby they can be challenging to resolve in wave flume experiments. Analogous conclusions can be drawn from the numerical computations by Gramstad *et al.*[5]

The probability density functions (PDFs) obtained before, on and past the depth transition are reported in Figure 6. As expected, only marginal departures from the Gaussian distribution are visible in the deep region, whereas near the depth transition PDFs display heavy tails for positive elevations which are progressively enhanced by increasing the depth transition, and represent a clear signature of rogue-wave events. In the shallow region, PDFs settle on a markedly asymmetric shape, but no longer exhibit heavy tails.

We next focus on the evolution of the wave spectrum along the tank. Temporal power spectra are extracted from η time series after excluding the initial transient. The power spectra, reported in Figure 7, span up to ten decades in magnitude from the peak to the point where the tail is overwhelmed by numerical noise. The high-frequency noise, which is above machine-noise level, is mostly affected by the aforementioned interpolation scheme required to invert the conformal mapping. Figure 7 shows how the transition from the deep-water to the shallow-water regime reflects on the spectrum. The spectra associated to the transient state across the depth transition deviate dramatically from

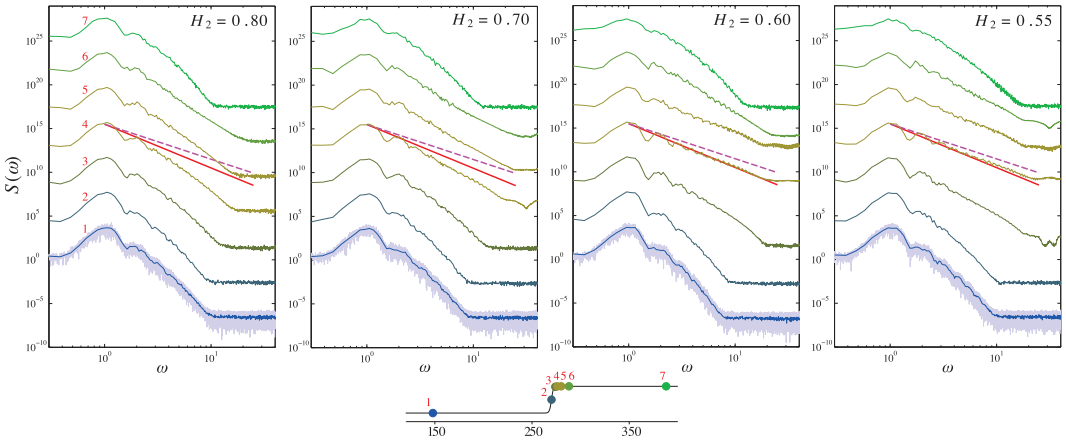

FIG. 7. Local power spectra of the surface elevation at the locations marked on the bathymetric profile sketched below (plots are progressively up-shifted by 10^4 from the previous one). Hamming window is applied to the time series before computing the spectra, and a smoothing filter is applied subsequently. The first spectrum from the bottom is shown both before (light-blue line) and after (dark-blue line) smoothing. The straight lines reference the ω^{-4} (dashed line) and ω^{-5} (solid line) power-laws.

both steady-state spectra. Near the depth transition the spectral tails decay much more slowly, and the two cases with the stronger depth transition exhibit marked consistency with Phillips ω^{-5} power-law, suggesting local formation of sharp-crested waves.[14] Note that the slow decaying spectral tails provide more high-frequency contribution to ω_p, which is consistent with the peaks observed in Fig. 4(a). Beyond the depth variation, the spectrum settles rapidly on the equilibrium state, which, as expected, is broader banded than it is in the deep side.

In closing, the results presented in this paper provide a detailed description of the response of a progressive, random wave field to a strong depth variation. After validating our procedure against available experimental data, we have focused on four cases characterized by the same nearly deep-water dynamics ($H_1 = 1.8$, $k_pH_1 \approx 1.8$) in the deep side of the tank, and intermediate-depth ($H_2 = 0.8$, $k_pH_2 \approx 1.03$) to near shallow-water ($H_2 = 0.55$, $k_pH_2 \approx 0.78$) regimes in the shallow side. In doing so, we focused on conditions outside the realm of validity of the Boussinesq and KdV models employed in previous studies. We have shown the growing intensity of extreme-wave activity for increasing depth variations, in a region localized around the depth variation. Such transition region bridges two different statistical equilibria, and is strongly affected by non-equilibrium dynamics.

We further stress that, in the recent literature, studies are growing numerous which emphasize the link between extreme-wave activity and spectral settling. Examples can be drawn from a number of different contexts and regimes, such as: developing modulational instability,[15,16] random crossing-sea,[17] and bathymetric variations.[3,6] Our results contribute to reinforce a unifying viewpoint on rogue wave dynamics, in which extreme waves are seen as a footprint of non-equilibrium dynamics, regardless of the specific factor imposing a shift of the statistical equilibrium.

This research was supported by the European Research Council under the research Project No. ERC-2011-AdG 290562-MULTIWAVE and Science Foundation Ireland under Grant No. SFI/12/ERC/E2227.

[1] K. Dysthe, H. E. Krogstad, and P. Müller, "Oceanic rogue waves," Annu. Rev. Fluid Mech. **40**, 287–310 (2008).
[2] C. Kharif and E. Pelinovsky, "Physical mechanisms of the rogue wave phenomenon," Eur. J. Mech. B/Fluids **22**, 603–634 (2003).
[3] K. Trulsen, H. Zeng, and O. Gramstad, "Laboratory evidence of freak waves provoked by non-uniform bathymetry," Phys. Fluids **24**, 097101 (2012).
[4] H. Zeng and K. Trulsen, "Evolution of skewness and kurtosis of weakly nonlinear unidirectional waves over a sloping bottom," Nat. Hazards Earth Syst. Sci. **12**, 631–638 (2012).
[5] O. Gramstad, H. Zeng, K. Trulsen, and G. K. Pedersen, "Freak waves in weakly nonlinear unidirectional wave trains over a sloping bottom in shallow water," Phys. Fluids **25**, 122103 (2013).
[6] A. Sergeeva, E. Pelinovsky, and T. Talipova, "Nonlinear random wave fields in shallow water: Variable Korteweg-de Vries framework," Nat. Hazards Earth Syst. Sci. **11**, 323–330 (2011).
[7] C. Viotti, D. Dutykh, and F. Dias, "The conformal-mapping method for surface gravity wave in the presence of variable bathymetry and mean current," IUTAM Proc. **11**, 110–118 (2014).
[8] C. Viotti, D. Dutykh, and F. Dias, "Emergence of coherent wave groups in deep-water random sea," Phys. Rev. E **87**, 063001 (2013).
[9] P. A. E. M. Janssen and M. Onorato, "The intermediate water depth limit of the Zakharov equation and consequences for wave prediction," J. Phys. Ocean. **37**, 2389–2400 (2007).
[10] Z. Tian, M. Perlin, and W. Choi, "Frequency spectra evolution of two-dimensional focusing wave groups in finite depth water," J. Fluid Mech. **688**, 169–194 (2011).
[11] L. Shemer, A. Sergeeva, and D. Liberzon, "Effect of the initial spectrum on the spatial evolution of statistics of unidirectional nonlinear random waves," J. Geophys. Res. **115**, C12039, doi:10.1029/2010JC006326 (2010).
[12] M. Onorato, A. L. Osborne, M. Serio, L. Cavalieri, C. Brandini, and C. T. Stansberg, "Observation of strongly non-gaussian statistics for random sea surface gravity waves in wave flume experiments," Phys. Rev. E **70**, 067302 (2004).
[13] G. B. Whitham, "Mass, momentum and energy flux in water waves," J. Fluid Mech. **12**, 135–147 (1962).
[14] S. Nazarenko, S. Lukaschuk, S. McLelland, and P. Denissenko, "Statistics of surface gravity wave turbulence in the space and time domains," J. Fluid Mech. **642**, 395–420 (2010).
[15] W. Xiao, Y. Liu, G. Wu, and D. K. P. Yue, "Rogue wave occurrence and dynamics by direct simulations of nonlinear wave-field evolution," J. Fluid Mech. **720**, 357–392 (2013).
[16] H. Socquet-Juglard, K. Dysthe, K. Trulsen, H. E. Krogstad, and J. Liu, "Probability distributions of surface gravity waves during spectral changes," J. Fluid Mech. **542**, 195–216 (2005).
[17] A. Toffoli, E. M. Bitner-Gregersen, A. R. Osborne, M. Serio, J. Monbaliu, and M. Onorato, "Extreme waves in random crossing seas: Laboratory experiments and numerical simulations," Geophys. Res. Lett. **38**, L06605, doi:10.1029/2011GL046827 (2011).